Journal of Molecular Structure 1136 (2017) 69–79

Contents lists available at ScienceDirect

Journal of Molecular Structure

journal homepage: http://www.elsevier.com/locate/molstruc

Substitution effect on a hydroxylated chalcone: Conformational, topological and theoretical studies

Jean M.F. Custodio [a], Wesley F. Vaz [b], Fabiano M. de Andrade [c], Ademir J. Camargo [a], Guilherme R. Oliveira [c], Hamilton B. Napolitano [a, *]

[a] Ciências Exatas e Tecnológicas, Universidade Estadual de Goiás, Anápolis, GO, Brazil
[b] Instituto Federal de Educação, Ciência e Tecnologia de Mato Grosso, Lucas do Rio Verde, MT, Brazil
[c] Instituto de Química, Universidade Federal de Goiás, Goiânia, GO, Brazil

ARTICLE INFO

Article history:
Received 10 October 2016
Received in revised form
25 January 2017
Accepted 27 January 2017
Available online 30 January 2017

Keywords:
Hydroxylated chalcone
Hirshfeld surface
DFT

ABSTRACT

The effect of substituents on two hydroxylated chalcones was studied in this work. The first chalcone, with a dimethylamine group (HY-DAC) and the second, with three methoxy groups (HY-TRI) were synthesized and crystallized from ethanol on centrosymmetric space group $P2_1/c$. The geometric parameters and supramolecular arrangement for both structures obtained from single crystal X-ray diffraction data were analyzed. The intermolecular interactions were investigated by Hirshfeld surfaces with their respective 2D plot for quantification of each type of contact. Additionally, the observed interactions were characterized by QTAIM analysis, and DFT calculations were applied for theoretical vibrational spectra, localization and quantification of frontier orbitals and potential electrostatic map. The flatness of both structures was affected by the substituents, which led to different monoclinic crystalline packing. The calculated harmonic vibrational frequencies and homo-lumo gap confirmed the stability of the structures, while intermolecular interactions were confirmed by potential electrostatic map and QTAIM analysis.

1. Introduction

Chalcones have attracted much attention in the scientific community due to their multifunctional basic skeleton. Basically, they are formed by an olefin portion and a carbonyl group that bind two substituted aromatic rings, providing a delocalized π system [1–4]. The broad features of these compounds, such as materials applied to environmental science [5–9] and biological activities [3,10–17], are results of their natural origin which allows for a wide range of chemical compositions derived from this basic skeleton. Furthermore, the understanding of the structure-activity relationship has motivated the synthetic production of chalcones that possess the desired chemical, physical and biological properties [18].

As a result, hydroxylated chalcones have been thoroughly studied, and many results show desirable properties related to this group [19–21]. As environmental agents, these chalcones would act as defense against UV radiation and as protection against oxidative stress. Furthermore, these compounds could be involved in various physiological processes such as defense against bioaggressors, redox homeostasis and dissipation of excess excitation energy [22]. As biological agents, Hofmann et al. [23] state that a minimum of three hydroxyl groups was a requirement of effective xanthine oxidase inhibition. In addition, two hydroxyl groups at neighboring positions on at least one phenyl ring were responsible for effective radical scavenging, which makes hydroxylated chalcones interesting candidates as possible agents for the treatment of hyperuricemia. A QSAR study made by Silva et al. [24] shows that the presence of a hydroxyl group in *ortho* position increased activities against *S. mutans*, while its absence or OH in *meta* position decreased the activity.

However, unlike previous studies that assessed the effect of the chemical composition on the biological activities, we propose a comparative structural study of two hydroxylated chalcones in order to relate the chemical, physical and biological properties of these compounds to structural factors, such as flatness, bond angles and intermolecular interactions. The first, a dimethylamine-hydroxychalcone, is used as a ratiometric fluorescent probe for the detection of alkaline phosphatase (ALP), an indicator of several

* Corresponding author.
E-mail address: hbnapolitano@gmail.com (H.B. Napolitano).

http://dx.doi.org/10.1016/j.molstruc.2017.01.076
0022-2860/

diseases, such as hepatitis, prostate cancer, osteoporosis and bone tumor [25–28]. The second chalcone is a trimethoxy-hydroxychalcone with chemical composition similar to the first, excepting only the substituents of the second ring, which enabled this study. We synthesized both chalcones and studied their structures from single crystal X-ray diffraction. In addition, we performed theoretical calculations in order to assess the vibrational frequencies, nucleophilic attack sites and chemical stability for both structures.

2. Methodology

2.1. Synthesis and crystallization

To a solution of aromatic aldehyde (2 mmol) and aromatic ketone (2 mmol) in 8.0 mL of ethanol, an amount of 1.0 mL of 24% sodium hydroxide in water at 10 °C was added. After stirring overnight at room temperature, the reaction medium was neutralized with 10% HCl. The solid was filtered and recrystallized from ethanol.

2.2. Crystallographic characterization

A single crystal of each compound was carefully selected under polarizing microscope in order to perform its structural analysis by X-ray diffraction. The crystals were collected at room temperature using a Bruker APEX II CCD diffractometer with graphite-monochromated MoKa radiation (λ = 0.71073 Å). The structure was solved by direct methods and refined by full-matrix least squares on F^2 using SHELXL2014 software [29]. HY-DAC crystallized in the monoclinic crystal system and space group P21/c [30] with the following unit cell metrics: a = 12.124 Å, b = 10.275 Å, c = 12.506 Å; α = 90°, β = 115.87°, γ = 90° and V = 1401.8 Å^3. HY-TRI also crystallized in the monoclinic crystal system and space group P21/c [30] with the following unit cell metrics: a = 12.687 Å, b = 8.586 Å, c = 15.349 Å; α = 90°, β = 107.99°, γ = 90° and V = 1549.9 Å^3. In both structures, H atoms connected to aromatic carbon atoms were placed at calculated positions and refined as riding, with C—H = 0.94 Å and Uiso(H) = 1.2Ueq(C). H atoms attached to N and O atoms, and CH_3 group, were located reliably on difference Fourier maps, and their positions were refined as riding on their parent atoms, with Uiso(H) = 1.2Ueq(N) and Uiso(H) = 1.5Ueq (C or O). Mercury [31] and Crystal Explorer 3.1 [32] were used to generate molecular representations, tables and pictures. The possible intermolecular interactions and hydrogen bond were checked by PARST software [33] and studied from the Hirshfeld surface. The crystallographic information files of $C_{17}H_{17}NO$ (HY-DAC) and $C_{18}H_{17}O_5$ (HY-TRI) molecule were deposited in the Cambridge Structural Database [34] under the codes CCDC 1507796 and 1507797, respectively.

2.3. Hirshfeld surface analysis

The potential intermolecular interactions of HY-DAC and HY-TRI were visualized and interpreted using Hirshfeld surface (HS) analysis. The idea for HS appeared from an attempt to define the space occupied by a molecule in a crystal intending to partition the crystal electron density into molecular fragments [35]. F. L. Hirshfeld defined a weight function for each atom in a molecule as

$$w_a(r) = \rho_a^{at}(\boldsymbol{r}) \Big/ \sum_{i \in molecule} \rho_i^{at}(\boldsymbol{r}) \quad (1)$$

where $\rho_i^{at}(r)$ are spherically averaged electron densities of the various atoms. Then, the electron density of an atomic fragment can be defined as

$$\rho_a(\boldsymbol{r}) = w_a(\boldsymbol{r})\rho^{mol}(\boldsymbol{r}) \quad (2)$$

where $\rho^{mol}(\boldsymbol{r})$ indicates the molecular electron density. Crystal Explorer 3.1 [32] software has been widely used to obtain several properties that can be viewed in HS. Among these properties we have the distance of atoms external (d_e) and internal (d_i), to the surface. This information can be represented in 3D or 2D histograms known as fingerprints. The Crystal Explorer 3.1[32] program normalizes these distances (d_{norm}) using the van der Waals radius of the appropriate internal and external atom of the surface [36].

$$d_{norm} = \left(d_i - r_i^{vdw}\right) \Big/ r_i^{vdw} + \left(d_e - r_e^{vdw}\right) \Big/ r_e^{vdw} \quad (3)$$

The graphical representation of d_{norm} allows us to identify a particular intermolecular interaction via a color coding system. Red and blue colors in the HS are associated with shorter and longer distances than van der Waals intermolecular contacts, respectively [37]. The surfaces were mapped for HY-DAC and HY-TRI as a function of d_e and d_i by Crystal Explorer 3.1 [32] software, and for the fingerprint we used the standard 0.6–2.8 Å view of d_e vs. d_i.

2.4. Computational procedure

The start geometries for HY-DAC and HY-TRI optimizations in gas phase were taken from X-ray data as described before. All computation procedures present in this work were carried out using the Gaussian09 [38] package of programs. The hybrid functional of Truhlar and Zhao, M06-2X [39], with 6–311 + g (d) basis set and B3LYP [40] exchange-correlation functionals with 6–311 g (d,p) [41,42] basis set were applied to calculate the geometric and electronic properties of the compounds. The M06-2X functional is a nonlocal functional parametrized for nonmetals with double the amount of nonlocal exchange [39]. This functional is recommended for noncovalent interaction such as C—H···O and C—H···π [43–45]. The optimizations of geometric parameters were carried out without constraint and to confirm if the optimized geometry found in local minimum analytic harmonic frequency calculations had been carried out using the same level of theory. With the support of potential energy distribution (PED) analysis in Veda 4 [46] software and the animation option of Gaussview [47], the assignments of the vibrational frequencies were made.

3. Results and discussion

3.1. Crystallographic structure

Our crystallographic data collected for (E)-3-(4-(dimethylamino)phenyl)-1-(2-hydroxyphenyl)prop-2-en-1-one (HY-DAC) are very similar to those found by Zhiqiang Liu and coworkers [28], with monoclinic crystal system, $P2_1/c$ space group and unit cell parameters a = 12.124 Å, b = 10.275 Å, c = 12.506 Å and β = 115.87°, showing one molecule per asymmetric unit. Similarly, (E)-1-(2-hydroxyphenyl)-3-(3,4,5-trimethoxyphenyl)prop-2-en-1-one (HY-TRI) also crystallized with a single molecule per asymmetric unit in a $P2_1/c$ space group and monoclinic crystal system, with metrics a = 12.687 Å, b = 8.586 Å, c = 15.394 Å and β = 15.394°, like those found by Hui Wu, Zhou Xua and Yong-Min Liang [48]. Complete data for HY-DAC and HY-TRI are shown in Table 1, followed by Ortep representations and an atom-numbering scheme for HY-DAC (Fig. 1a) and HY-TRI (Fig. 1b):

Excepting the substituted region, both structures are very similar in bond lengths and angles, as can be seen in Fig. 2a. Major

Table 1
Crystal data and structure refinement for HY-DAC and HY-TRI.

	HY-DAC		HY-TRI	
Empirical formula	$C_{17}H_{17}NO$		$C_{18}H_{17}O_5$	
Formula weight	267.31		313.32	
Temperature	293 (2) K			
Wavelength	0.71073 Å			
Crystal system, space group	Monoclinic, $P2_1/c$		Monoclinic, $P2_1/c$	
Unit cell dimensions	a = 12.124 Å	α = 90°	a = 12.687 Å	α = 90°
	b = 10.275 Å	β = 115.87°	b = 8.586 Å	β = 107.99°
	c = 12.506 Å	γ = 90°	c = 15.394 Å	γ = 90°
Volume	1401.8 $Å^3$		1594.9 $Å^3$	
Z, Calculated density	4, 1.267 Mg/m^3		4, 1.305 Mg/m^3	
Absorption coefficient	0.083 mm^{-1}		0.095 mm^{-1}	
F (000)	568		660	
Theta range for data collection	1.867–25.360°		1.688–25.385°	
Reflections collected/unique	7962/2568 [R (int) = 0.0202]		9745/2932 [R (int) = 0.0210]	
Completeness to theta = 25.242	100.0%		99.8%	
Refinement method	Full-matrix least-squares on F^2			
Data/restraints/parameters	2568/0/186		2932/0/212	
Goodness-of-fit on F^2	1.040		1.037	
Final R indices [I > 2sigma(I)]	R1 = 0.0376, w*R*2 = 0.1002		R1 = 0.0373, w*R*2 = 0.0904	
R indices (all data)	R1 = 0.0523, w*R*2 = 0.1115		R1 = 0.0528, w*R*2 = 0.1011	

discrepancies are observed in angles C10–C15–C14 and C10–C11–C12 (122.76° and 122.30° for HY-DAC and 120.30° and 120.13° for HY-TRI). Electronic effects explain this difference: HY-DAC has an activating group ($N(CH_3)_2$), resulting in a positive partial charge around the C15 and C11 atom. Although HY-TRI also has an activating group (OCH_3), the *orto*-substitution increases the electronic density and decrease the angles of *meta*-position, compared to HY-DAC. In addition, molecular planarity evidences the structural differences. HY-DAC is flatter than HY-TRI, with the largest deviations from planarity involving the dihedral angles C11–C10–C9–C8 and O2–C7–C8–C9, present in the carbonyl and olefin regions (2.97° and 3.81°, respectively). Comparing only the

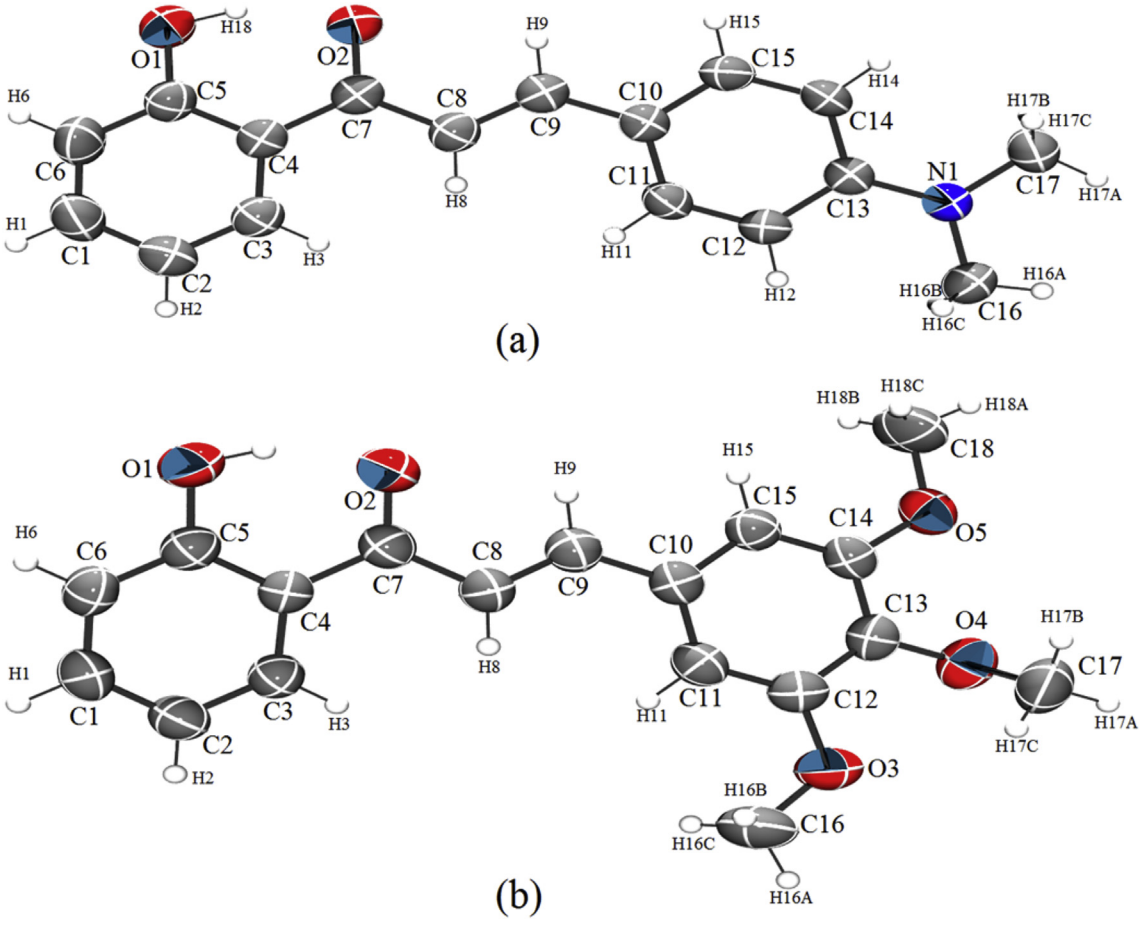

Fig. 1. The ORTEP diagram of ellipsoids at 50% probability level with the atomic numbering scheme for HY-DAC (a) and HY-TRI (b).

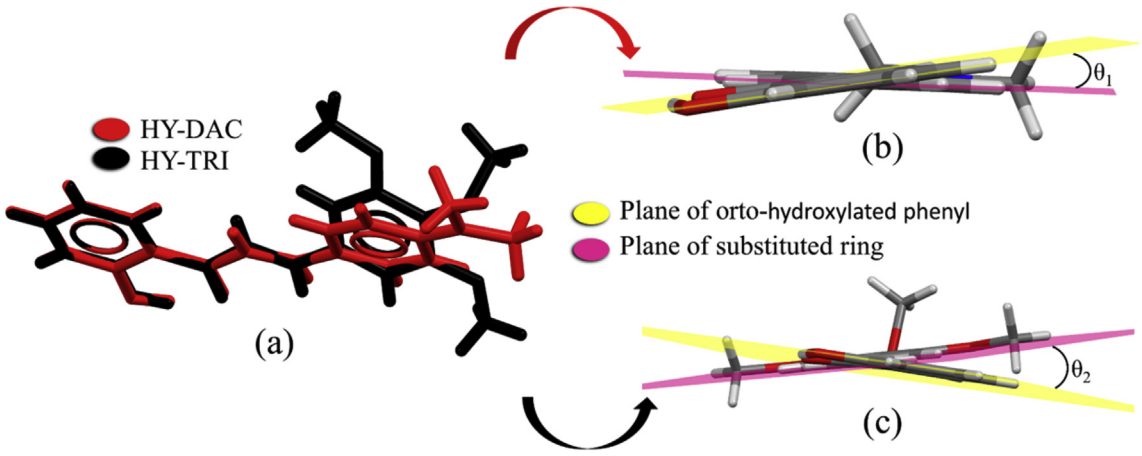

Fig. 2. Overlapping of HY-DAC and HY-TRI (a); Representation of dihedral angles formed by planes of aromatic rings of HY-DAC (b) and HY-TRI (b). $\theta_1 = 10.24°$ and $\theta_2 = 15.22°$.

regions in common of HY-DAC and HY-TRI, the dihedral angles C5–C4–C7–O2, C3–C4–C7–C8, O2–C7–C8–C9 are evidence of low planarity of HY-TRI, with values of −4.62°, −6.92° and −6.94°. Fig. 2 also shows the angle formed by planes of aromatic rings of HY-DAC (Fig. 2b) and HY-TRI (Fig. 2c). In the presence of the dimethylamine substituent, aromatic rings has a deviation $\theta_1 = 10.24°$, increased to $\theta_2 = 15.22°$ when methoxy groups are bonded at positions 3, 4 and 5 of the phenyl ring. In total, changes in the substitution pattern are responsible for an angular difference between the aromatic rings of HY-DAC and HY-TRI equal to 24.84°.

Regarding inter/intramolecular interactions, the HY-TRI compound has more interactions than HY-DAC. The crystal packing of HY-DAC is stabilized by one strong intramolecular H-bond involving O1–H18···O2 and one non-classical intermolecular interaction involving C3–H3···O1, which contributes to the zigzag repetition in the direction of the *c* axis. In addition to the strong H-bond O1–H19···O2, the spatial arrangement of HY-TRI also resembles a zigzag chain along the *b* axis, involving C–H···O and C–H···C interactions. While only one interaction contributes to this chain in HY-DAC, HY-TRI is stabilized by C9–H9···C6, C1–H1···O2, C3–H3···O5 and C3–H3···C14 interactions. Two factors explain the HY-TRI interactions: the increased electron density caused by the three methoxy substituents in HY-TRI allows the C3–H3···C14 and C3–H3···O5 interactions, and the angular difference between the aromatic rings of HY-DAC and HY-TRI brings HY-TRI molecules closer together and allows C9–H9···C6 and C1–H1···O2 interactions, causing an increase in the calculated density for HY-TRI. Information about distance, angles and the symmetry code of total interactions of HY-DAC and HY-TRI is shown in Table 2, followed by a representation of interactions and packing, in Fig. 3.

The topological analysis of crystal is as important as the molecular structural study, because it involves the arrangement of the molecular units in the crystalline environment. We evaluated the neighborhood pattern by Hirshfeld surface analysis. The first approach involves distances between components of crystal: d_e is the distance from an external molecule to the Hirshfeld surface, while d_i is the distance from an internal nucleus to the Hirshfeld surface [49]. Hence, high values for d_i indicate donor regions of intermolecular contacts and high values for d_e indicate acceptor regions of intermolecular contacts [35]. Intermolecular interactions of HY-DAC are presented in Fig. 4a, followed by intermolecular interactions of HY-TRI, in Fig. 4b and c. Such surfaces are composed of a color scale where blue indicates low intensity and red indicates high intensity of contacts. In Fig. 4 a, (1) and (2) are the places with high intensity of d_i and d_e of C3–H3···O1 interaction. In contrast, for HY-TRI, donor regions of C9–H9···C6, C1–H1···O2, C3–H3···O5 and C3–H3···C14 interactions are recognized as the red points in (3), (6), (9) and (10), while (4), (5), (7) and (8) represent acceptor regions of these interactions. Note that the red points (8) and (10) are higher than other points of HY-TRI, indicating that C3–H3···C14 interaction is stronger than C9–H9···C6, C1–H1···O2 and C3–H3···O5 interactions.

Hirshfeld surfaces are a very effective tool for the recognition of intermolecular interactions by evaluating not only classical and non-classical hydrogen bond, but also hydrophobic interactions (π···π and C–H···π interactions). These interactions are important for the three-dimensional arrangement of the compounds studied here and have characteristic features in the Hirshfeld surface shape index. We evaluated the π interactions involved in the crystal packing of HY-DAC and HY-TRI, and the results are illustrated in Fig. 5. HY-DAC is stabilized by both π···π and C–H···π interactions (Fig. 5a). The π···π interaction, involving only Cg1 (the gravity center of the aromatic ring formed by C10, C11, C12, C13 and C15 atoms) is separated by a distance of 4.014 Å and recognized by two triangular shapes above the aromatic ring, indicating the place where two molecules meet (Fig. 5b). Fig. 5c shows the effect of C–H···π interactions involving Cg1 and Cg2 (gravity center of aromatic ring formed by C1, C2, C3, C4, C5 and C6 atoms) in the Hirshfeld surface shape index: π systems involved in C16–H16B···Cg1 [H16B···Cg1 = 3.383 Å, D-H···A = 104.79°] and C17–H17C···Cg2 [H16B···Cg1 = 3.105 Å, D-H···A = 113.12°] cause large depressions above the aromatic ring, seen as large red regions of concave curvature [50,51]. In contrast, HY-TRI is stabilized by only one C–H···π involving Cg3 (the gravity center of the aromatic ring formed by C10, C11, C12, C13 and C15 atoms), C2 and H2 atoms [H2···Cg3 = 2.838 Å, D-H···A = 142.69°] (Fig. 5d). The same

Table 2
Total intra/intermolecular interactions for HY-DAC and HY-TRI.

D-H···A	d (D-H)Å	d (H···A)Å	d (D···A)Å	d (DH···A) (°)	Type
HY-DAC					
O1–H18···O2	0.961	1.613	2.509	153.31	Intra
C3–H3···O1 (i)	0.931	2.665	3.523	153.73	Inter
HY-TRI					
O1–H19···O2	0.944	1.643	2.523	153.40	Intra
C9–H9···C6 (i)	0.930	2.872	3.736	155.11	Inter
C1–H1···O2 (ii)	0.931	2.648	3.381	136.15	Inter
C3–H3···O5 (iii)	0.930	2.687	3.546	153.91	Inter
C3–H3···C14 (iii)	0.930	2.802	3.503	133.01	Inter

(i) = x,1/2-y,1/2 + z; (ii) = x,1/2-y,-1/2 + z; (iii) = x,3/2-y,-1/2 + z.

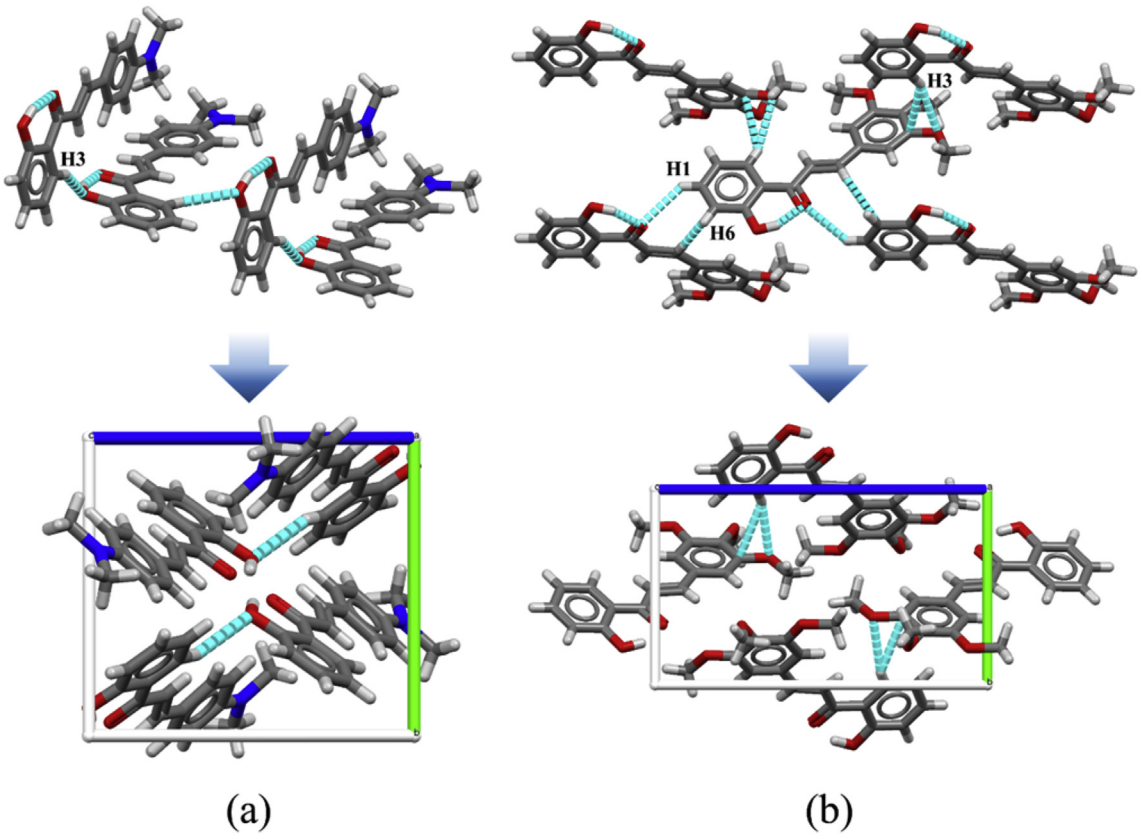

Fig. 3. Representation of total interactions and crystal packing of HY-DAC (a) and HY-TRI (b).

features already discussed for the C–H···π interactions of HY-DAC were observed for HY-TRI.

The combination of distance functions d_i and d_e provides various pieces of information about the system studied [52]. This combination is called a fingerprint and summarizes all interactions in a 2D plot created by binning (d_i, d_e) pairs in intervals of 0.01 Å

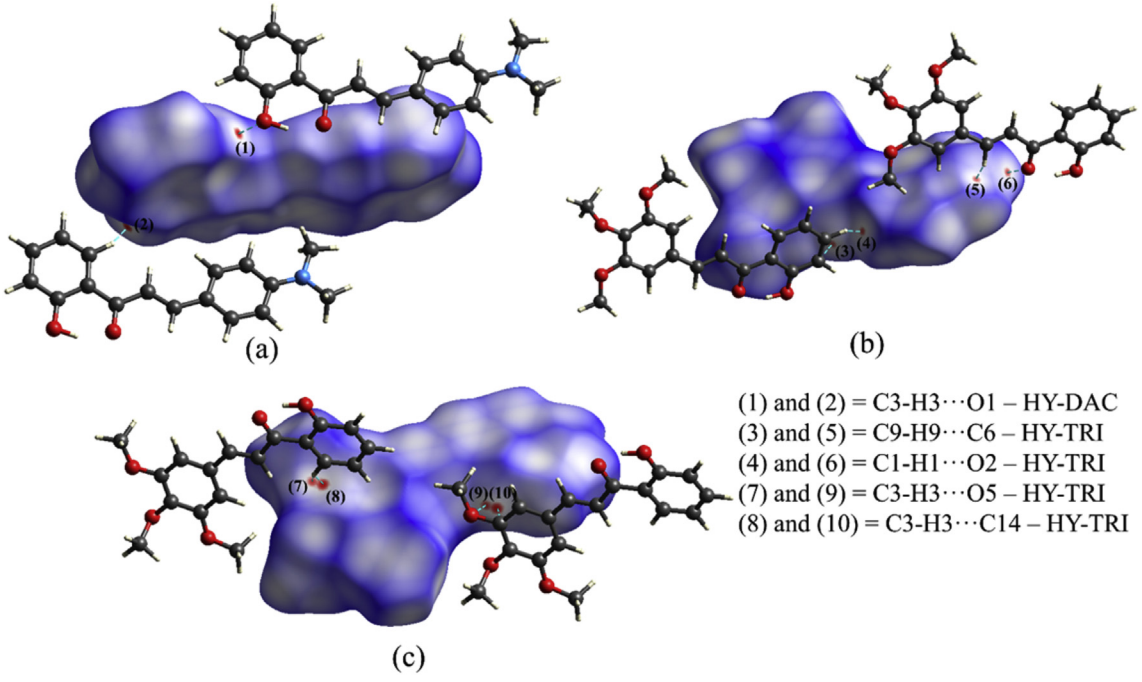

Fig. 4. Hirshfeld surfaces indicating intermolecular interactions of HY-DAC (a) and HY-TRI (b) e (c). Interactions are represented by dotted blue lines.

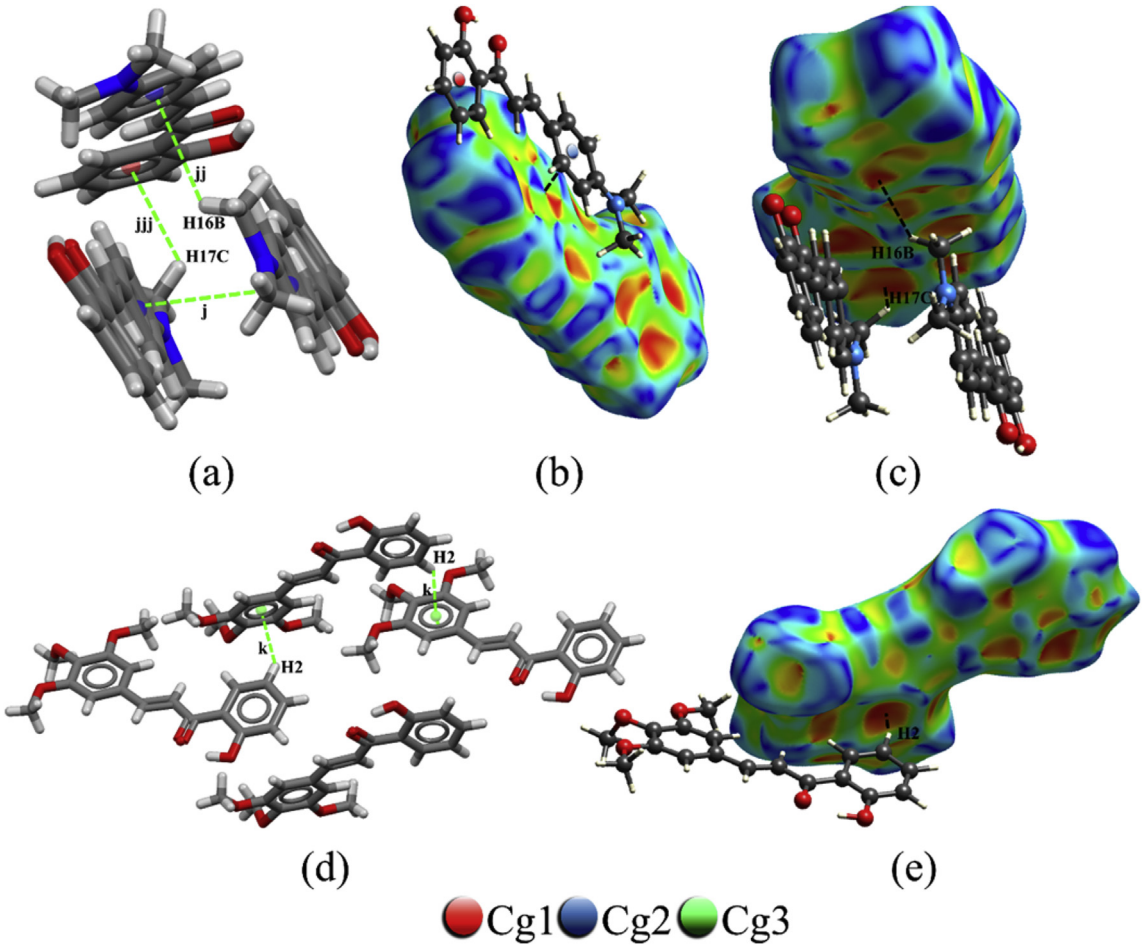

Fig. 5. Representation of π···π and C–H···π interactions of HY-DAC (a) and HY-TRI (b). Hirshfeld surface shape index of HY-DAC evidencing the π···π (c) and C–H···π (d) interactions and HY-TRI, revealing the C–H···π (e) interaction.

and coloring each bin of the resulting 2D histogram as a function of the fraction of surface points in that bin, in a color scale from blue (few points) through green to red (many points) [51,53,54]. Fig. 6a shows the percentage of each contact for HY-DAC and HY-TRI, followed by their respective fingerprint plots in Fig. 6b and c.

Due to the substitution pattern, HY-TRI has more O···H contact than HY-DAC. This difference is noted as a higher intensity region with d_e and d_i ranging from 1.2 to 2.0 Å in Fig. 6c. Generally, O···H contacts are represented by two peaks in fingerprints, where the upper peak ($d_e > 1.4$ Å and $d_i < 1.4$ Å) is the donor regions and the lower peak ($d_e < 1.4$ Å and $d_i > 1.4$ Å) is the acceptor regions. The C9–H9···C6 interaction in HY-TRI is responsible for the main difference between H···H contacts of both structures. It is recognized as blue points with coordinates $d_e \approx 1.3$ Å; $d_i \approx 1.1$ Å and $d_e \approx 1.1$ Å; $d_i \approx 1.3$ in the HY-TRI fingerprint. For both structures, C···H contacts have a wing shape in fingerprints and are related to C–H···π interactions. This shape is very similar to HY-DAC and HY-TRI, except for two peaks in $d_e \approx 1.8$–2.0 Å; $d_i \approx 1.2$ Å and $d_e \approx 1.2$ Å; $d_i \approx 1.8$–2.0 Å in HY-TRI, caused by C2–H2···Cg3 interaction. Finally, totally absent in HY-TRI, the HY-DAC fingerprint shows an intensity in $d_e \approx d_i \approx 1.8$ Å, indicating the place where the aromatic rings of π··· π interaction overlap.

The Quantum Theory of Atoms in Molecules (QTAIM) is a quantitative and qualitative approach by which host–guest interactions can be easily analyzed. QTAIM represents an advance in the evaluation of molecular properties in chemical compounds independent of their nature. One of its advantages, when compared to techniques with the same purpose, is the non-restriction of origin of the electron density of the evaluated system. This means that QTAIM does not depend only on electron densities calculated by *ab initio* or DFT methodologies, but can be grounded in electronic systems experimentally obtained via X-ray diffraction [38,55,56]. Qualitatively, a chemical bond/interaction is defined in terms of the electron density ρ and its gradient vector ∇ρ. The gradient vector represents the direction of greater variation of the electron density, and when its value is zero at one point, it is said that there is a maximum electron density at that point, called the critical point [57]. Based on this assumption, we confirm the existence of intermolecular interactions already discussed by the location of the Bond Critical Point (BCP) by Laplacian electron density $\nabla^2\rho$ [58–61]. Although Hirshfeld surfaces indicate the C3–H3···C14 interaction in HY-TRI, this interaction is not found by QTAIM analysis. The bond critical points found for HY-DAC and HY-TRI are represented in Fig. 7a and Fig. 7b, respectively:

Besides the distance, another parameter that classifies an interaction as weak, strong or very strong is its energy. By studying the energy of a hydrogen bond [X–H···O (X = C, N, O)], Espinosa, Molins, and Lecomte [62] determined that

$$E_{HB} = \frac{V\left(r_{bcp}\right)}{2} \tag{4}$$

where E_{HB} = Energy hydrogen bond and $V(r_{bcp})$ = Energy Density potential in the corresponding BCP. Each BCP has a value for the

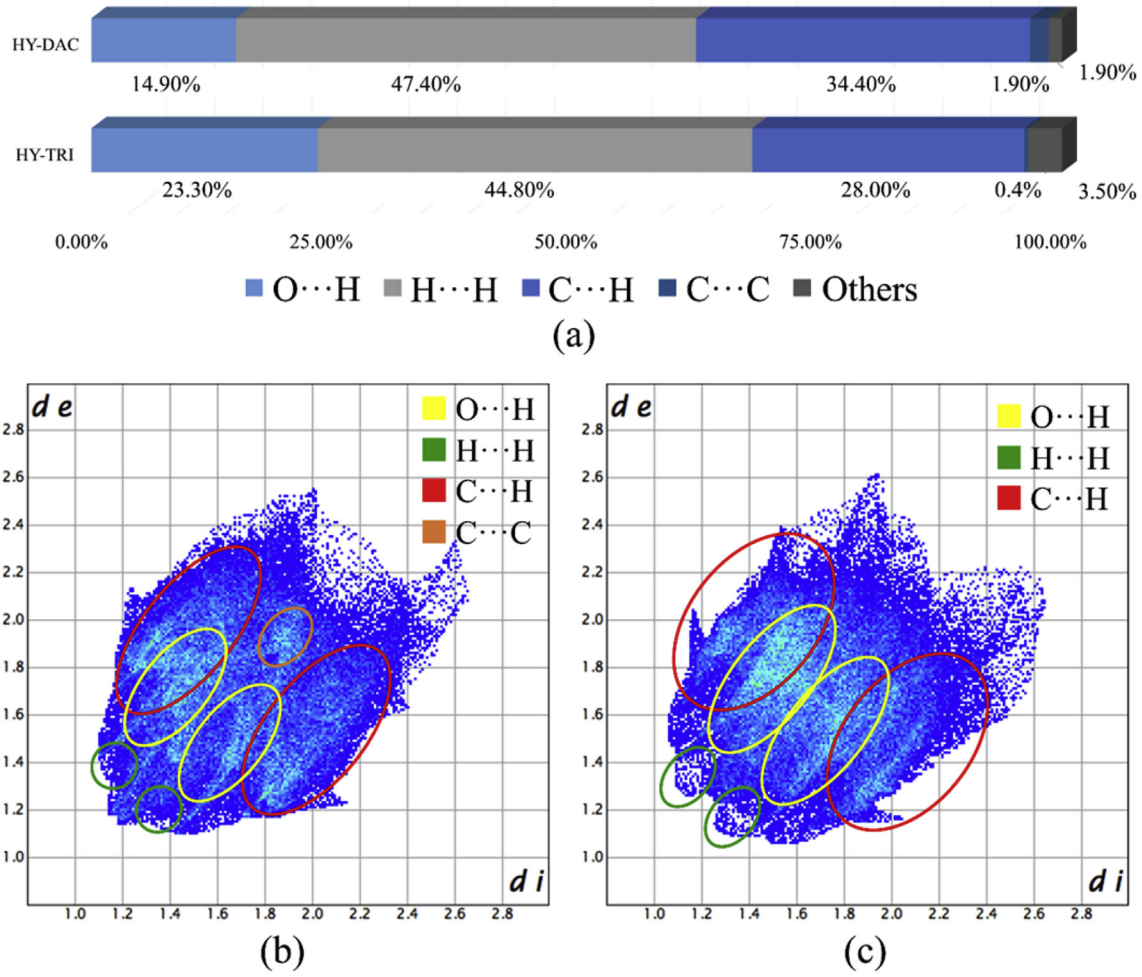

Fig. 6. Quantifying the different types of contacts in HY-DAC and HY-TRI (a) followed by fingerprints for HY-DAC (b) and HY-TRI (c).

potential energy density calculated by the Multiwfn program [63], which provides calculation of the hydrogen bond energy by replacing it in Equation (4), resulting in Table 3:

Note that the intramolecular H bond is stronger in HY-TRI than HY-DAC. This decrease in energy is caused by the C3—H3···O1 interaction that acts on the oxygen involved in intramolecular interaction. Finally, the positive values for the Laplacian critical point classifies the HY-DAC and HY-TRI interactions as closed-shell type.

3.2. Theoretical characterization

Our major aim in the theoretical analysis in this work was to quantify the effect of substituting the three methoxy groups from

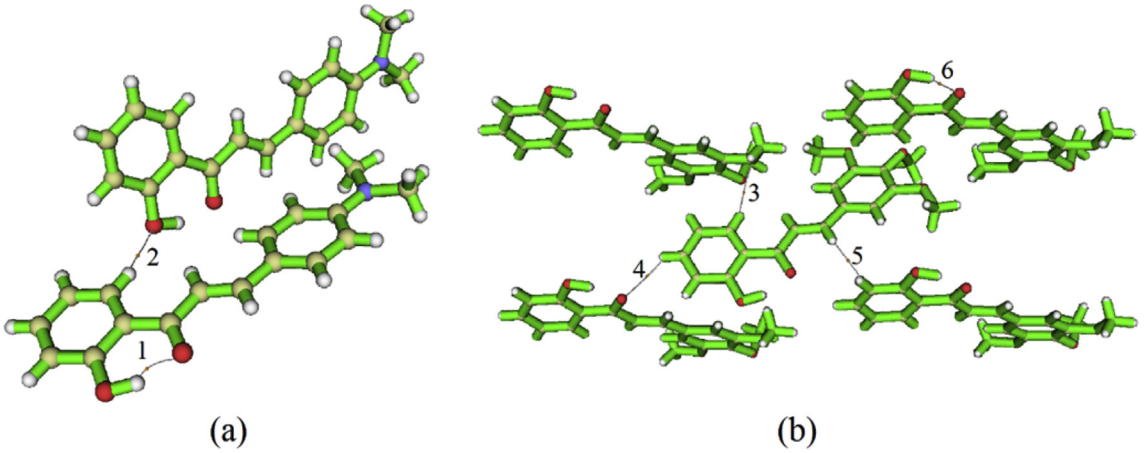

Fig. 7. Representation of bond critical points of HY-DAC (a) and HY-TRI (b).

Table 3
Topological parameters calculated by quantum theory of atoms in molecules (QTAIM). BCP = Bond critical point; V (r_{bcp}) = Potential energy density; E_{HB} = Bond energy; ∇ [2]ρ Laplacian critical point; au = atomic units = 627.5095 kcal mol^{-1}.

	BCP	V (r_{bcp}) (au)	E_{HB} (Kcal/mol)	$\nabla^2\rho$ (au)	Interaction
HY-DAC	1	−0.072207325800	−22.65539039	0.013277360211	O1–H18···O2
	2	−0.009417884996	−2.954906014	0.013737317860	C3–H3···O1
HY-TRI	3	−0.003756927443	−1.178753775	0.022182122460	C3–H3···O5
	4	−0.003787432061	−1.188324744	0.023234850860	C1–H1···O2
	5	−0.002299879157	−0.721597976	0.015578557070	C9–H9···C6
	6	−0.058952248280	−18.49654705	0.179433609100	O1–H19···O2

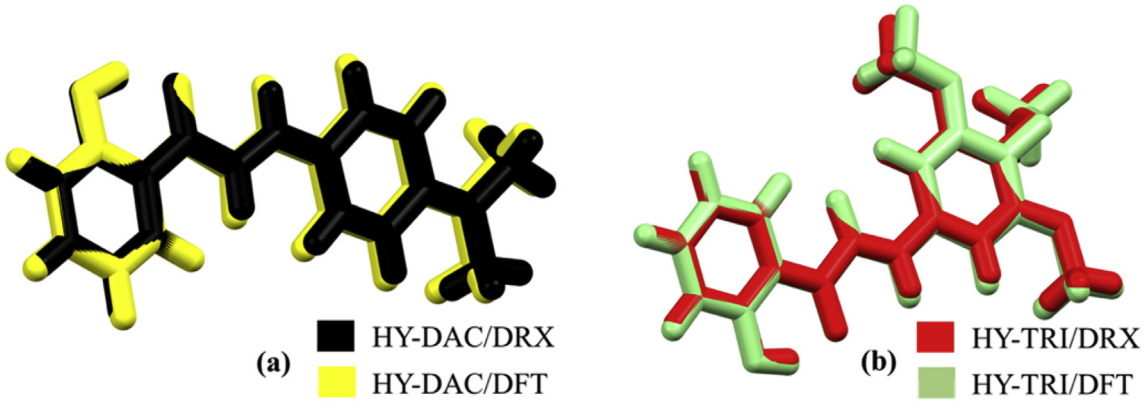

Fig. 8. Overlapping of experimental and theoretical (M062X) structures of HY-DAC (a) and HY-TRI (b).

HY-TRI by the amine group from HY-DAC. We studied the effect of the molecular interactions theoretically, in solid state, in the geometric parameters of HY-DAC. Since optimized geometry was carried out in gas phase, we can conclude that the structural variations observed between optimized and experimental structures are a consequence of the molecular interactions in the solid state phase. Structurally, the largest deviations from planarity between the solid and the gas phase of HY-DAC are shown in the dihedral angles involving C4–C5–O1–H18, C14–C13–N1–C17, C8=C9–C10–C11 and C9=C8–C7 = O2. For HY-TRI, deviations from planarity are observed near to carbonyl-olefin, olefin-hydroxylated aromatic, methoxyl and hydroxyl regions. Fig. 8 shows graphically the main differences between theoretical and experimental structures by overlapping the models, while Table S1 (Supplementary Information) shows bond lengths and bond angles:

Based on the values in S1, we calculated the roots of the mean squared errors (RMSE) for bond lengths and bond angles parameters, obtained with M062X functional, for both molecules. HY-DAC presents a RMSE of 21.70° (11.37° with B3LYP) for the bond angles and 0.0027 Å (0.0032 Å with B3LYP) for bond lengths, while HY-TRI presents 7.65° (10.34° with B3LYP) and 0.0030 Å (0.0038 Å with B3LYP), respectively, for the same parameters. This shows that HY-TRI has a better agreement with bond angles, whereas for bond lengths, HY-DAC has the closest values. Hence, although containing more interactions, the conformation in gas phase of HY-TRI is less affected by intermolecular interactions in solid state than HY-DAC.

3.3. Vibrational assignments

Table 4 shows the theoretical vibrational frequencies for the proposed compounds. For the sake of clarity, we decided to discuss only the values for the main absorbing groups. As can be seen in Table 4, these values are in line with each other and between the expected experimental values, according to the literature. In order to make a better comparison between theoretical and expected experimental results, we applied in the theoretical values a scaling factor of 0.947 [64] for M062X/6-311 + g (d,p) and a scaling factor of 0.966 [65] for the results obtained at B3LYP/6-311 g(d) level of theory. This procedure corrects the systematic overestimation of the vibrational frequencies that is characteristic of the DFT methods and, besides, makes it easier to carry out the assignments of the vibrational modes.

Experimentally, the OH stretching vibration mode, for phenols, shows strong centering bands ranging from 3400 cm^{-1} to 3300 cm^{-1}. The DFT calculations (M062X) give that band at 3216 cm^{-1} and 3236 cm^{-1} for HY-DAC and HY-TRI, respectively. These theoretical values, lower than expected, can be explained by the fact that, experimentally, the intermolecular hydrogen bonding weakens the O–H bond, thereby shifting the band to lower frequency [66]. The strong C–OH single-bond stretching vibrations are observed in the range from 1260 cm^{-1} to 1000 cm^{-1}; phenols give that absorption at about 1220 cm^{-1} because of conjugation of the oxygen with the ring, which shifts the band to higher energy [66]. The bands at 1282 cm^{-1} and 1285 cm^{-1}, to HY-DAC and HY-TRI, respectively, in DFT calculations, are assigned as stretching C–OH mode. The carbonyl group absorbs strongly in the range from 1850 cm^{-1} to 1650 cm^{-1}. In chalcones we must consider the conjugation effects that increase the single bond character of the C=O and C=C bonds in the resonance hybrid and hence lower their force constants, resulting in a lowering of the absorption frequencies. Generally, this effect results in a 25 cm^{-1} to 45 cm^{-1} lowering of the carbonyl frequency [66]. These calculated frequencies are 1643 cm^{-1} for HY-DAC and 1651 cm^{-1} for HY-TRI. Silver and Boykin [67] studied the effect of the substituents on the carbonyl stretching frequency of chalcones and observed that when there is the *p*-dimethylamine group, just like in HY-DAC, the value of this stretching is 1558 cm^{-1}. For chalcones with methoxy group, just like in HY-TRI, C=O stretching occurs, on average, around 1585 cm^{-1}. The stretching modes of the vinyl group occur at 1660 cm^{-1}-1600 cm^{-1}, but conjugation often moves C=C

Table 4
Vibrational assignments, experimental and calculated wavenumbers in cm^{-1} of HY-DAC and HY-TRI.

IR Assignments	B3LYP unscaled IR freq.	M062X unscaled IR freq.	B3LYP scaled IR freq.	M062X scaled IR freq.	B3LYP I	M062X I
ν OH	(a)3292.73	(a) 3396.26	3180.78	3216.26	494.99	621.90
	(b)3318.68	(b) 3418.05	3205.84	3236.89	418.43	529.87
ν C–OH	(a)1346.27	(a) 1354.77	1300.50	1282.97	13.74	19.32
	(b)1330.03	(b) 1356.91	1284.81	1285.00	292.07	54.08
ν C=O	(a) 1601.03	(a) 1646.08	1546.59	1558.84	840.97	494.67
	(b) 1693.20	(b) 1674.43	1635.63	1585.68	316.97	417.79
ν C=C	(a)1687.50	(a) 1734.99	1630.13	1643.03	273.62	312.30
	(b)1607.98	(b) 1743.51	1553.31	1651.10	392.48	261.40
ν_{sym}CH3	(a) 3006.83	(a) 3023.76	2904.60	2863.50	119.11	67.65
	(b)3023.88; 3012.77; 3011.95	(b) 3041.27; 3043.20; 3058.93	2921.06; 2910.33; 2909.54	2880.08; 2881.91; 2896.80	225.76	56.51
ν $_{asym}$CH3	(a)3146.19	(a) 3034.64; 3082.10	3039.22	2873.80; 2918.75	56.02	30.90
	(b)3136.55; 3144.97; 3145.50;	(b) 3113.93; 3133.34; 3168.42	3055.98; 3038.04; 3038.55	2948.89; 2967.27; 3000.49	140.56	24.28
ν C–N	(a) 1372.29	(a) 1379.84	1325.63	1306.71	23.37	47.25
ν O-C_{Aryl}	(b)944.05; 1268.27	(b) 975.11; 1307.09	911,95; 1225.14	923.42; 1238.19	345.01	232.04
ν O–C	(b)1030.45–1167.55	(b)1077.03–1208.13	995.41–1127.85	1019.94–1144.09	201.79	223.80

stretching into lower frequencies, that increases the intensity [66]. The calculated wavenumbers for this mode are 1643 cm^{-1} and 1651 cm^{-1} for HY-DAC and HY-TRI, respectively. The O–C stretching vibration of the O–CH_3 group appears in the wide 975 ± 125 cm^{-1} region with an intensity varying from weak to strong [68,69]. A methoxy group attached to an aromatic ring gives the asymmetric stretching in the range 1310–1210 cm^{-1} and symmetric stretching in the range 1050–1010 cm^{-1} [69]. The *ab initio* calculations give 1019 cm^{-1} and 1144 cm^{-1} as asymmetric and symmetric methoxy stretching vibrations, respectively. Electronic effects such as back-donation and induction, mainly caused by the presence of an oxygen atom adjacent to the methyl group, can shift the position of CH stretching mode. In aromatic methoxy compounds the asymmetric mode is expected in the region 2985 ± 20 cm^{-1} and 2955 ± 20 cm^{-1}, and the symmetric mode in the region 2845 ± 15 cm^{-1} [69]. For HY-DAC, the computed wavenumbers of asymmetric stretching of the CH_3 group appear in 2873 cm^{-1} and 2918 cm^{-1}, while the band in 2863 cm^{-1} is assigned as symmetric stretching mode. For HY-TRI, the computed wavenumbers of asymmetric stretching of the CH_3 group are 2948 cm^{-1}, 2967 cm^{-1} and 3000 cm^{-1}, while the bands in 2880 cm^{-1}, 2881 cm^{-1}; and 2896 cm^{-1} are assigned as symmetric stretching mode. The C–N absorption occurs at a higher frequency in aromatic amines because resonance increases the double-bond character between the ring and the attached nitrogen atom, so aromatic amines absorb from 1350 cm^{-1} to 1250 cm^{-1} [70]. Brouwer and Wilbrandt [71] found an IR band in 1344 cm^{-1} for C–N stretching in *N,N*-Dimethylaniline. Substitution in ring A with basic groups, $N(CH_3)_2$ and OCH_3, containing an unshared π-electron, result in bathochromic shifts of the longer wave length absorption band, and this effect is higher than for $N(CH_3)_2$ to OCH_3. This is understandable on the basis of partial electron withdrawal from the nitrogen. This propensity is offset by the inductive effect of the methyl group. The overall effect is that there is some lowering in the resonance contribution of the nitrogen lone pair towards the benzene ring of the chalcone molecule [72]. In this study, the C–N stretching occurs in 1306 cm^{-1} for HY-DAC and 923 cm^{-1} for HY-TRI.

3.4. Electrostatic potential surface

The molecular electrostatic potential (MEP) has been employed in characterizing various properties of chemical and biological systems. The electrostatic potential is a well-defined quantum-mechanical quantity, emphasizing the charge distribution of molecules three-dimensionally. It can also be explored experimentally through X-ray diffraction investigations [73,74]. The MEP surface with Mulliken atomic charges of HY-DAC and HY-TRI is shown in Fig. 9. The MEP contour map shows the negative red regions are more concentrated at the oxygen atoms on the electrophilic sites of both molecules. The positive blue regions are concentrated over the hydrogen atom attached to the nitrogen atom, for HY-DAC, and the methyl group, for HY-TRI, positioned on nucleophilic sites. The green region represents the zero potential of the title molecules. Thus, Fig. 9 confirms the existence of intra and intermolecular interactions of the title molecules in solid state. The dipole moment of the compound is another parameter that predicts the polarized nature of the molecule [75]. The theoretical study has shown that HY-DAC (7.8249D) has the highest values of dipole moments, thus it is more polarized, compared to those obtained for HY-TRI (3.1244D), while with B3LYP calculations these values are 8.2098 D and 3.5622 D, respectively. Through Mulliken atomic charges, we can see that the electron density on the carbonyl oxygen of HY-TRI

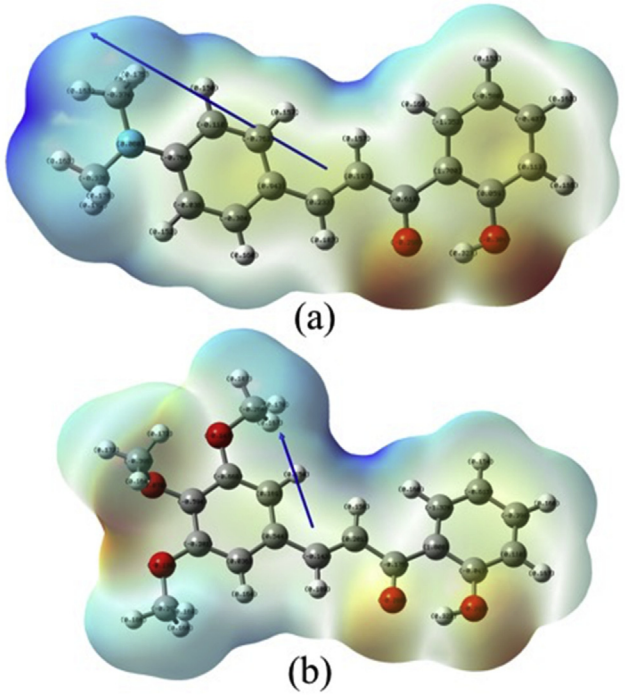

Fig. 9. Potential electrostatic surface calculated at M062X/6-311 + g (d,p) for HY-DCA (a) and HY-TRI (b) with Mulliken atomic charges. Electrostatic potential regions are represented in red while positive electrostatic potential areas are shown in dark blue. (For interpretation of the references to colour in this figure legend, the reader is referred to the web version of this article.)

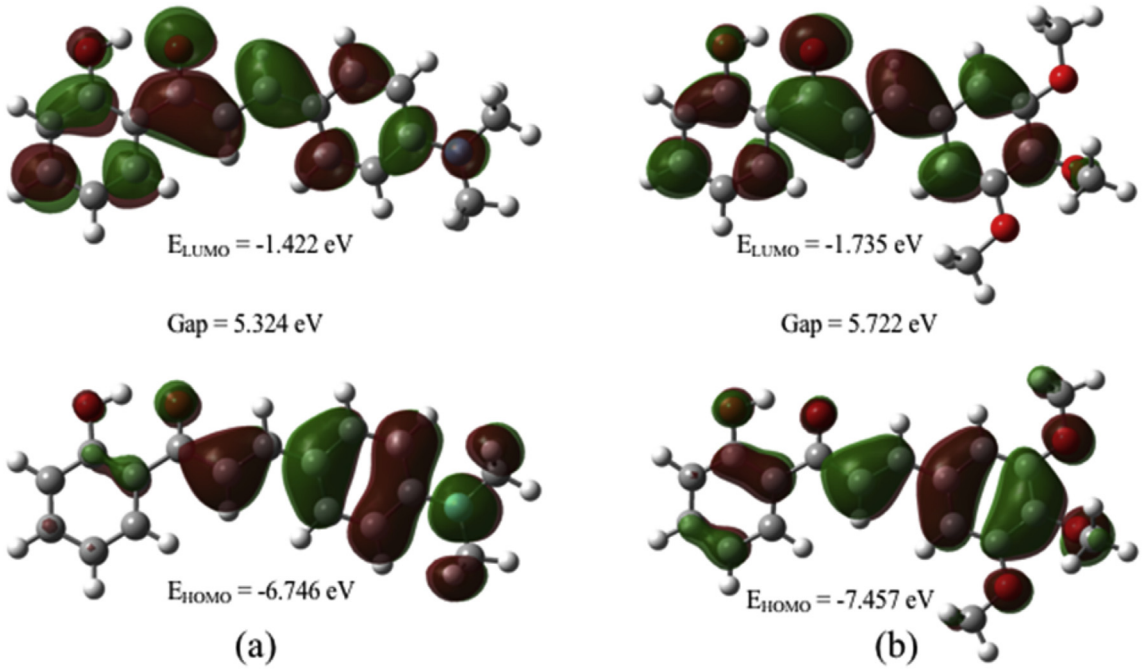

Fig. 10. The HOMO and LUMO distribution of HY-DCA (a) and HY-TRI (b) in gas-phase by using M062X.

(−7.86 eV) is slightly higher than that on HY-DAC (−8.13 eV). The negative charge on the oxygen atom of the hydroxy group in HY-DAC (−8.27 eV) is also lower compared to that of HY-TRI (−7.97 eV). On the other hand, it is observed that the positive values on the carbon atoms of the ring system in HY-TRI lead to a redistribution of electron density. Because of these strong positive charges, the carbon atoms of the HY-TRI ring where the oxygen atom is connected accommodate higher positive charges and become more acidic.

3.5. Frontier molecular orbitals

The Highest Occupied Molecular Orbital (HOMO) is the molecular orbital of highest energy that has electrons in it. The Lowest Unoccupied Molecular Orbital (LUMO) is the molecular orbital of lowest energy that does not have electrons in it. The energy difference (Gap) between the HOMO and the LUMO is related to the minimum energy needed to excite an electron in the molecule [76]. The band gap energy (i.e., the energy difference between the E_{LUMO} and E_{HOMO}) calculated for HY-DAC is 5.324 eV and 5.722 eV for HY-TRI. According to the frontier molecular orbital theory, chemical reactivity is strongly determined by the interaction of the HOMO and the LUMO of the reactants. The energy of HOMO is often associated with the electron donating ability of a molecule, and a higher HOMO energy value indicates a higher tendency of the molecule to donate electron(s) to the appropriate acceptor molecule with low energy and an empty/partially filled molecular orbital [77]. The HOMO/LUMO graphical surfaces of the studied compounds, calculated using M062X/6-311 + G (d,p) for HY-DAC and HY-TRI, are shown in Fig. 10. HY-TRI has a large HOMO-LUMO gap, which implies a high kinetic stability and low chemical reactivity, compared to HY-DAC. In all the structures, the HOMO is strongly delocalized on ring A and the double bond corresponding to the sites with the highest electron density. Absolute hardness (η) and softness (σ) are properties that also facilitate the analysis of the molecular reactivity and selectivity; a hard molecule has a large ΔE while a soft molecule has a small ΔE [77]. The global chemical hardness (η) is a measure of the resistance of an atom to a charge transfer. The chemical softness (σ) describes the capacity of an atom or group of atoms to receive electrons [78], and both parameters were calculated in this work. The η for HY-DAC is 2.662 eV and the σ is 0.3756 eV, while the η for HY-TRI is 2.861 eV and the σ is 0.3495 eV. Thus, we conclude that HY-DAC has a higher capacity to receive electrons, while HY-TRI has a higher capacity to resist a charge transference (i.e, resistance to changing its electronic configuration).

4. Conclusions

Due to the smaller number of intermolecular interactions, HY-DAC is more planar than HY-TRI, which can be measured by the angle formed between the planes of the aromatic rings. Hence, the twists present in HY-TRI added to the electron density of the methoxy groups provide a closer contact between their molecules when compared to HY-DAC. In contrast, the planar character of HY-DAC allows its stability through π···π and C–H···π interactions.

Geometry optimization was carried out using the DFT (M062X and B3LYP) method of the Gaussian 09 software package with 6-311 + G (d,p) and 6-311G(d) basis sets. The calculated harmonic vibrational frequencies confirm the stability of the structures, and the main absorbing groups are characterized. RMSDs for bond angles and bond lengths in HY-DAC and HY-TRI are, respectively, 21.70°, 0.0027 Å, 7.65° and 0.0030 Å. MEP confirms the existence of intra and intermolecular interactions of the title molecules in solid state. HY-TRI has a large HOMO-LUMO gap, which implies a high kinetic stability and low chemical reactivity, compared to HY-DAC. Analyzing the Hardness and Softness, we conclude that HY-DAC has a higher capacity to receive electrons, while HY-TRI has a higher capacity to resist changing its electronic configuration.

Acknowledgements

The authors are grateful to Conselho Nacional de Desenvolvimento Científico e Tecnológico (Grant no. 313070/2014-8) and

Coordenação de Aperfeiçoamento de Pessoal de Nível Superior for financial support and to Prof. Felipe Terra Martins, of the Department of Chemistry of the Federal University of Goias, for the X-ray data collection.

Appendix A. Supplementary data

Supplementary data related to this article can be found at http://dx.doi.org/10.1016/j.molstruc.2017.01.076.

References

[1] V. Yerragunta, T. Kumaraswamy, D. Suman, V. Anusha, P. Patil, T. Samhitha, PharmaTutor 1 (2013) 54–59.
[2] C.B. Patil, S.K. Mahajan, S.A. Katti, J. Pharm. Sci. Res. 1 (2009) 11–22.
[3] M.J. Matos, S. Vazquez-Rodriguez, E. Uriarte, L. Santana, Expert Opin. Ther. Pat. 25 (2015) 351–366.
[4] B.E. Aksöz, R. Ertan, I. Şalkon, Y. Özellikleri, Fabad J. Pharm. Sci. (2013) 223–242.
[5] T.T.H. Dao, H.J.M. Linthorst, V.R, Phytochem. Rev. (2011) 397–412.
[6] D.-T.C.E. Graña, M.J. Reigosa, A.M. Sánchez-Moreiras, Planta Daninha, Viçosa-MG 34 (2016) 607–616.
[7] P.G. Mahajan, D.P. Bhopate, G.B. Kolekar, Shivajirao R. Patil, J. Lumin. Appl. 2 (2015) 1–13.
[8] K. Velmurugan, J. Prabhu, L. Tang, T. Chidambaram, M. Noel, S. Radhakrishnan, R. Nandhakumar, Anal. Methods 6 (2014) 2883–2888.
[9] W. Yang, Z. Cheng, Y. Xu, J. Shao, W. Zhou, J. Xie, M. Li, New J. Chem. 39 (2015) 7488–7494.
[10] P. O. Patil and S. B. Bari, 2013, 2013, 1–8.
[11] M. a Rahman, Chem. Sci. J. (2011) 2011. CSJ-29.
[12] Z. Nowakowska, Eur. J. Med. Chem. 42 (2007) 125–137.
[13] D.K. Mahapatra, S.K. Bharti, V. Asati, Eur. J. Med. Chem. 98 (2015) 69–114.
[14] D.K. Mahapatra, V. Asati, S.K. Bharti, Eur. J. Med. Chem. 92 (2015) 839–865.
[15] R. Ghosh, A. Das, World J. Pharm. Pharm. Sci. 3 (2014) 578–595.
[16] Noor-Jahan Farah-Saeed, M. Ahmad Mehjabeen, Afr. J. Pharm. Pharmacol. 9 (2015) 367–374.
[17] P. Rani, N. Kumar, P. Sharma, D. Kishore, Int. J. Chem. Pharm. Sci. 4 (2013) 19–24.
[18] G.R. de Oliveira, H.C.B. de Oliveira, W.A. Silva, V.H.C. da Silva, J.R. Sabino, F.T. Martins, Struct. Chem. 23 (2012) 1667–1676.
[19] N. Sriwilaijaroen, M. Liu, M. Go and P. Wilairat, 2006, 37, 607–612..
[20] M. Liu, P. Wilairat, M. Go, J. Med. Chem. 44 (2001) 4443–4452.
[21] V. Ramkumar, S. Anandhi, P. Kannan, R. Gopalakrishnan, RSC Adv. 5 (2014) 586–596.
[22] M. Alejandra, M. Inés, G. Nuño, I. Catiana, A. Soledad, G. Inés, J. Esteban, M. Inés, Phytochem. Lett. 13 (2015) 134–140.
[23] E. Hofmann, J. Webster, T. Do, R. Kline, L. Snider, Q. Hauser, G. Higginbottom, A. Campbell, L. Ma, S. Paula, Bioorg. Med. Chem. 24 (4) (2015) 578–587.
[24] W.A. Silva, C.K.Z. Andrade, H.B. Napolitano, I. Vencato, C. Lariucci, M.M.R.C. De Castro, A.J. Camargo, J. Braz. Chem. Soc. 24 (2013) 133–144.
[25] H. Zhang, X. Cheng, K. Wang, S. Huang, H. Zhang, Y. Wang, Angew. Chem. Int. Ed. 54 (2015) 8369–8373.
[26] Z. Song, R.T.K. Kwok, E. Zhao, Z. He, Y. Hong, J.W.Y. Lam, B. Liu, B.Z. Tang, ACS Appl. Mater. Interfaces 6 (2014) 17245–17254.
[27] L. Ma, Y. Sun, D. Cao, H. Chen, Z. Liu, Q. Fang, Spectrochim. Acta Part A Mol. Biomol. Spectrosc. 103 (2013) 120–124.
[28] Z. Liu, Q. Fang, W. Yu, G. Xue, D. Cao, M. Jiang, Acta Crystallogr. Sect. C Cryst. Struct. Commun. 58 (2002) 445–446.
[29] G.M. Sheldrick, Acta Crystallogr. Sect. C Struct. Chem. 71 (2015) 3–8.
[30] P. Paufler, Acta Crystallogr. Sect. A 60 (2004) 641–642.
[31] C.F. Macrae, I.J. Bruno, J. a. Chisholm, P.R. Edgington, P. McCabe, E. Pidcock, L. Rodriguez-Monge, R. Taylor, J. van de Streek, P. a. Wood, J. Appl. Crystallogr. 41 (2008) 466–470.
[32] S.K. Wolff, D.J. Grimwood, J.J. McKinnon, M.J. Turner, D. Jayatilaka, M.A. Spackman, Crystal Explorer (Version 3.1), University of Western Australia, 2012.
[33] M. Nardelli, J. Appl. Crystallogr. 28 (1995) 659.
[34] C.R. Groom, F.H. Allen, Angew. Chem. Int. Ed. 53 (2014) 662–671.
[35] M.A. Spackman, D. Jayatilaka, CrystEngComm 11 (2009) 19–32.
[36] S. Soudani, V. Ferretti, C. Jelsch, F. Lefebvre, C. Ben Nasr, Inorg. Chem. Commun. 61 (2015) 187–192.
[37] Z. Yousefi, H. Eshtiagh-Hosseini, A. Salimi, A. Janiak, J. Mol. Struct. 1083 (2015) 460–470.
[38] M.J. Frisch, G.W. Trucks, H.B. Schlegel, G.E. Scuseria, M.A. Robb, J.R. Cheeseman, G. Scalmani, V. Barone, B. Mennucci, G.A. Petersson, H. Nakatsuji, M. Caricato, X. Li, H.P. Hratchian, A.F. Izmaylov, J. Bloino, G. Zheng, J.L. Sonnenberg, M. Hada, M. Ehara, K. Toyota, R. Fukuda, J. Hasegawa, M. Ishida, T. Nakajima, Y. Honda, O. Kitao, H. Nakai, T. Vreven, J.A. Montgomery Jr., J.E. Peralta, F. Ogliaro, M. Bearpark, J.J. Heyd, E. Brothers, K.N. Kudin, V.N. Staroverov, R. Kobayashi, J. Normand, K. Raghavachari, A. Rendell, J.C. Burant, S.S. Iyengar, J. Tomasi, M. Cossi, N. Rega, J.M. Millam, M. Klene, J.E. Knox, J.B. Cross, V. Bakken, C. Adamo, J. Jaramillo, R. Gomperts, R.E. Stratmann, O. Yazyev, A.J. Austin, R. Cammi, C. Pomelli, J.W. Ochterski, R.L. Martin, K. Morokuma, V.G. Zakrzewski, G.A. Voth, P. Salvador, J.J. Dannenberg, S. Dapprich, A.D. Daniels, Ö. Farkas, J.B. Foresman, J.V. Ortiz, J. Cioslowski, D.J. Fox, Gaussian Inc. Wallingford CT (2009) 34 (Wallingford CT).
[39] Y. Zhao, D.G. Truhlar, Theor. Chem. Acc. 120 (2008) 215–241.
[40] A.D. Becke, J. Chem. Phys. 98 (1993) 5648.
[41] A.D. McLean, G.S. Chandler, J. Chem. Phys. 72 (1980) 5639.
[42] R. Krishnan, J.S. Binkley, R. Seeger, J.A. Pople, J. Chem. Phys. 72 (1980) 650.
[43] J. López-López, R. Ayala, J. Mol. Liq. 220 (2016) 970–982.
[44] K.E. Riley, M. Pitonák, P. Jurecka, P. Hobza, Chem. Rev. 110 (2010) 5023–5063.
[45] E.G. Hohenstein, S.T. Chill, C.D. Sherrill, J. Chem. Theory Comput. 4 (2008) 1996–2000.
[46] M.H. Jamroz, Vibrational Energy Distribution Analysis VEDA 4, Warsaw, 2010.
[47] R. Dennington, T. Keith, J. Millam, GaussView, Version 5, Semichem Inc., Shawnee Mission, KS, 2009.
[48] H. Wu, Z. Xu, Y.-M. Liang, Acta Crystallogr. Sect. E Struct. Rep. Online 61 (2005) o1434–o1435.
[49] S. Madan Kumar, B.C. Manjunath, G.S. Lingaraju, M.M.M. Abdoh, M.P. Sadashiva, N.K. Lokanath, Cryst. Struct. Theory Appl. 2 (2013) 124–131.
[50] S.A. Hosseini, G. Mahmoudi, P. Garczarek, P. Hazendonk, M. Abedi, M. Servati Gargari, J. Mol. Struct. 1105 (2016) 159–168.
[51] J.J. McKinnon, M. a. Spackman, A.S. Mitchell, Novel Tools for Visualizing and Exploring Intermolecular Interactions in Molecular Crystals, vol. 60, 2004.
[52] W.F. Vaz, J.M.F. Custodio, R.G. Silveira, A.N. Castro, E.M. Campos, M.M. Anjos, G.R. Oliveira, C. Valverde, H.B. Napolitano, RSC Adv. Int. J. Furth. Chem. Sci. (2016) 79215–79227.
[53] M. a Spackman, J.J. McKinnon, Crystengcomm 4 (2002) 378–392.
[54] A.D. Martin, J. Britton, T.L. Easun, A.J. Blake, W. Lewis, M. Schröder, Cryst. Growth Des. 15 (2015) 1697–1706.
[55] R.F.W. Bader, Chem. Rev. 91 (1991) 893–928.
[56] P. Belanzoni, P.S. Carvalho, J.E. Theodoro, O.H. Thiemann, J. Ellena, H.B. Napolitano, J. Struct. Chem. 55 (2014) 1596–1606.
[57] B.G. Oliveira, R.C.M.U. Araújo, M.N. Ramos, Quim. Nova 33 (2010) 1155–1162.
[58] S. Hati, D. Datta, J. Comput. Chem. 13 (1992) 912–918.
[59] M. Palusiak, S.J. Grabowski, J. Chem. Res. 2004 (2004) 492–493.
[60] S.E. O'Brien, P.L. Popelier, Can. J. Chem. 77 (1999) 28–36.
[61] P.L.A. Popelier, J. Phys. Chem. A 103 (1999) 2883–2890.
[62] E. Espinosa, E. Molins, C. Lecomte, Chem. Phys. Lett. 285 (1998) 170–173.
[63] T. Lu, F. Chen, J. Comput. Chem. 33 (2012) 580–592.
[64] R.D. Johnson III, NIST Computational Chemistry Comparision and Benchmark Data Base, IOP Publishing web, 2013 (Accessed 27 Dez 2016), http://cccbdb.nist.gov/vibscale2.asp?method=58&basis=1.
[65] R.D. Johnson III, NIST Computational Chemistry Comparision and Benchmark Data Base, IOP Publishing web, 2013 (Accessed 27 Dez 2016), http://cccbdb.nist.gov/vibscale2.asp?method=8&basis=7.
[66] D.L. Pavia, G.M. Lampman, G.S. Kriz, J.A. Vyvyan, Introduction to Spectroscopy, fifth ed., Cengage Learning, Mason, Ohio, 2015.
[67] N.L. Silver, D.W. Boykin, J. Org. Chem. 35 (1970) 759–764.
[68] A. Raj, K. Raju, H.T. Varghese, C.M. Granadeiro, H.I.S. Nogueira, C. Yohannan Panicker, J. Braz. Chem. Soc. 20 (2009) 549–559.
[69] C.Y. Panicker, H.T. Varghese, M.A. John, B. Harikumar, Orient. J. Chem. 24 (2008) 973–976.
[70] G. Raja, K. Saravanan, S. Sivakumar, Elixir Comp. Chem. 44 (2012) 7341–7346.
[71] A. Brouwer, R. Wilbrandt, J. Phys. Chem. 3654 (1996) 9678–9688.
[72] D.N. Dhar, D.V. Singhal, Spectrochim. Acta Part A Mol. Spectrosc. 26 (1982) 1171–1172.
[73] B. Galabov, V. Nikolova, S. Ilieva, Chem. A Eur. J. 19 (2013) 5149–5155.
[74] A. Dhandapani, S. Manivarman, S. Subashchandrabose, J. Mol. Struct. 1127 (2016) 212–225.
[75] G. Gece, Corros. Rev. 33 (2015) 195–202.
[76] T.E. Brown, H.E.H. LeMay, B.E. Bursten, C. Murphy, Chemistry the Central Science, thirteenth ed., Pearson, New York, 2014.
[77] B. Ramaganthan, M. Gopiraman, L.O. Olasunkanmi, M.M. Kabanda, S. Yesudass, I. Bahadur, A.S. Adekunle, I.B. Obot, E.E. Ebenso, RSC Adv. 5 (2015) 76675–76688.
[78] R.G. Parr, R.G. Pearson, J. Am. Chem. Soc. 105 (1983) 7512–7516.